Published OnlineFirst August 19, 2011; DOI:10.1158/0008-5472.CAN-11-1020

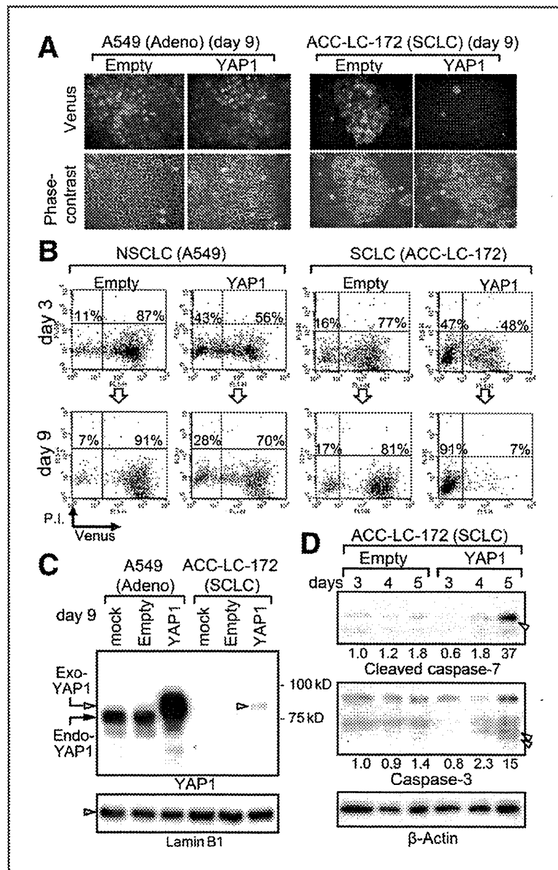

Figure 5. Lineage-dependent growth-regulating effects of YAP1 in lung cancers. A, fluorescent image of lentivirus-infected A549 and ACC-LC-172 obtained 9 days after infection. Cells were infected with a YAP1-expressing or empty lentivirus carrying the fluorescent protein Venus. YAP1 and empty virus infection resulted in fluorescent signals in A549 cells. In contrast, fluorescence-positive cells were scarcely detected in ACC-LC-172 cells infected with the YAP1-virus, whereas noninfected cells grew well. B, flow cytometric analysis of fluorescence-positive cells. Lentivirus-infected cells were analyzed at 3 and 9 days after infection. The fluorescence-positive population was moderately increased in the A549 cells infected with the YAP1-virus, whereas that population almost disappeared in ACC-LC-172 cells infected with the YAP1-virus. C, Western blotting analysis of YAP1. A549 abundantly expressed endogenous and exogenous (HA-tagged) YAP1. In contrast, ACC-LC-172 did not express endogenous YAP1. In addition, exogenous YAP1 was scarcely detected. D, Western blotting analysis of caspases. Five days after infection, activated cleavage of caspase-7 and caspase-3 was detected in YAP1 virus-infected ACC-LC-172 cells. Normalized intensities of cleaved caspases are numerically indicated.

blotting analysis, using lysates harvested on day 9, which showed scarcely detectable HA-tagged exogenous YAP1 protein expression in ACC-LC-172 as opposed to the abundant exogenous YAP1 expression in A549 cells (Fig. 5C). Cleavage of caspase-7 and caspase-3 was detected in YAP1-introduced ACC-LC-172 cells (Fig. 5D), whereas propidium iodide–stained dead cells were frequently observed in YAP1-introduced fluorescence-positive cells in ACC-LC-172 (Supplementary Fig. S6B), but not in A549 (data not shown). YAP1 introduction also resulted in growth suppression in 2 other SCLC cell lines, NCI-H69 and ACC-LC-48 (Supplementary Fig. S7), which confirmed the results observed in ACC-LC-172.

Discussion

The present results clearly show that ASH1 directly transactivates *miR-375*, resulting in an NE lineage-specific upregulation of *miR-375* in lung cancers. Although NeuroD1 and Pdx1 potentially bind to the E-box in the *miR-375* promoter (13), their expression was rarely detected and showed no correlations with *miR-375* expression (data not shown). Therefore, we believe that ASH1 plays a major role as a transcriptional activator of *miR-375*. Our finding of NEB-specific expression of *miR-375* also supports the existence of an ASH1–*miR-375* signaling axis in the lung. It is important to note that *miR-375* was recently reported to be detectable in pancreatic islet cells under the regulation of NeuroD1 and Pdx1, as well as in pituitary and adrenal glands (13–16). Herein, we clearly showed the functional importance of 3 E-boxes (E1, E2, and E3) in ASH1-mediated induction of the promoter activity of *miR-375*. Furthermore, a recent report described the promoter activity of a similar genomic region 5′ to murine *miR-375* in a β-cell line, though its responsiveness to potential activators such as NeuroD1 and ASH1 was not examined (17).

Downregulation of *miR-375* has been reported in a few other types of cancer (18–20). Interestingly, *miR-375* was suggested to play tumor suppressor roles in those cancer types, whereas target genes for *miR-375* thus far reported include PDK1, 14-3-3ζ (19), HuD (21), and JAK2 (22). Also, hepatocellular carcinoma was recently added to the list of cancers with *miR-375* downregulation and YAP1 has been suggested to be a target gene relieved by that downregulation. Consistent with those findings, we observed moderate downregulation of PDK1, 14-3-3ζ, HuD, and JAK2 when *miR-375* was introduced to A549 cells, though YAP1 showed the most significant downregulation in our experimental settings (Supplementary Fig. S8B). In addition, we did not observe clear growth inhibition of A549 cells stably introduced with a lentivirus expressing *miR-375* (Supplementary Fig. S8A), even though YAP1 was effectively downregulated by *miR-375* (Fig. 4B–D). Along this line, it is notable that *miR-375* knockout mice were shown to be hyperglycemic in association with decreased β-cell mass as a result of impaired proliferation of β-cells (15) and that *miR-375* was shown to regulate a number of genes other than *YAP1*, which potentially control cellular growth and proliferation of pancreatic islets (15). It is also interesting that estrogen receptor-α (ERα)-expressing breast cancers showed ERα-signal dependency and a high expression of *miR-375* (23). ERα binds the *miR-375* promoter and induces its expression. *miR-375* in turn represses the *RAS, dexamethasone-induced 1* (*RASD1*) gene, which negatively regulates ERα expression, suggesting the existence of a positive feedback loop between ERα and *miR-375*, as well as a growth-promoting role of *miR-375* in ERα-positive breast cancers (23). Taken together, it is conceivable that *miR-375* plays distinct roles in various can-

Downloaded from cancerres.aacrjournals.org on February 26, 2012
Copyright © 2011 American Association for Cancer Research

Published OnlineFirst August 19, 2011; DOI:10.1158/0008-5472.CAN-11-1020

cers, depending on the cellular context and transcriptomes including its potential target genes, and that downregulation of YAP1 by ASH-1-transactivated *miR-375* promotes rather than inhibits growth of SCLC cells.

YAP1 has several domains including a TEAD binding region and 2 WW domains, whereas it lacks a DNA binding domain and functions as a transcriptional coactivator through interactions with DNA binding transcription factors (24–26). YAP1 interacts with the TEAD family through a TEAD binding domain, and transactivates growth-promoting genes, whereas it also binds to PPXY motif-containing molecules including p73 through WW domains, thus enhancing p73-dependent apoptosis in response to DNA damage (27–29). It has been reported that phosphorylation by AKT or repression by ΔNp63 downregulates the proapoptotic activity of YAP1 (30), and that PML is also involved in regulation of p73-YAP apoptotic signaling through sumoylation and stabilization of YAP (31). Therefore, accumulating evidence enhances the notion that YAP1 exerts both oncogenic and tumor-suppressive activities in a context-dependent manner (32, 33). The present findings show that YAP1 moderately promotes NSCLC proliferation when overexpressed, whereas it significantly suppresses SCLC growth, suggesting its lineage-dependent dual roles in lung cancers.

In conclusion, we identified *miR-375* as a direct transcriptional target for ASH1 and showed that it has a crucial role for mediating signals required for ASH1-mediated induction of NE features in lung cancers. In addition, the present findings indicate that *miR-375* directly downregulates YAP1, whereas we also found that it shows NE lineage-specific growth inhibitory activities in lung cancers. A future study of the downstream genes of the ASH1–*miR-375* axis will be of great interest to fully elucidate the underlying signaling networks involved in NE differentiation and highly malignant behaviors of NE lung cancers including SCLC.

Disclosure of Potential Conflicts of Interest

No potential conflicts of interest were disclosed.

Acknowledgments

We thank Dr. Hideki Murakami and Ms. Mika Yamamoto for their excellent technical help. We also thank Dr. H. Miyoshi (RIKEN BioResource Center) and Dr. A. Miyawaki (RIKEN Brain Science Institute) for generously providing the lentivirus vectors and Venus gene, respectively.

Grant Support

This work was supported in part by Grants-in-Aid for Scientific Research on Priority Areas and Scientific Research on Innovative Areas from the Ministry of Education, Culture, Sports, Science and Technology (MEXT) of Japan; grants-in-aid for Scientific Research (A) and (C) from the Japan Society for the Promotion of Science (JSPS); and grants-in-aid for Scientific Research from the Princess Takamatsu Cancer Research Fund, the Uehara Memorial Foundation and the Nagono Medical Foundation. E.Nishikawa was supported by a JSPS Research Fellowship.

The costs of publication of this article were defrayed in part by the payment of page charges. This article must therefore be hereby marked *advertisement* in accordance with 18 U.S.C. Section 1734 solely to indicate this fact.

Received March 23, 2011; revised August 4, 2011; accepted August 12, 2011; published OnlineFirst August 19, 2011.

References

1. Takahashi T, Sidransky D. Biology of lung cancer. In:Mason R, Broaddus V, Murray J, Nadel J, editors. Textbook of respiratory medicine. 4th ed. Philadelphia, PA: Elsevier Science; 2005. p. 1311–27.
2. Voortman J, Goto A, Mendiboure J, Sohn JJ, Schetter AJ, Saito M, et al. MicroRNA expression and clinical outcomes in patients treated with adjuvant chemotherapy after complete resection of non-small cell lung carcinoma. Cancer Res 2010;70:8288–98.
3. Du L, Schageman JJ, Irnov , Girard L, Hammond SM, Minna JD, et al. MicroRNA expression distinguishes SCLC from NSCLC lung tumor cells and suggests a possible pathological relationship between SCLCs and NSCLCs. J Exp Clin Cancer Res 2010;29:75.
4. Osada H, Takahashi T. MicroRNAs in biological processes and carcinogenesis. Carcinogenesis 2007;28:2–12.
5. Osada H, Takahashi T. let-7 and miR-17-92: small-sized major players in lung cancer development. Cancer Sci 2011;102:9–17.
6. Takamizawa J, Konishi H, Yanagisawa K, Tomida S, Osada H, Endoh H, et al. Reduced expression of the let-7 microRNAs in human lung cancers in association with shortened postoperative survival. Cancer Res 2004;64:3753–6.
7. Hayashita Y, Osada H, Tatematsu Y, Yamada H, Yanagisawa K, Tomida S, et al. A polycistronic microRNA cluster, miR-17-92, is overexpressed in human lung cancers and enhances cell proliferation. Cancer Res 2005;65:9628–32.
8. Matsubara H, Takeuchi T, Nishikawa E, Yanagisawa K, Hayashita Y, Ebi H, et al. Apoptosis induction by antisense oligonucleotides against miR-17-5p and miR-20a in lung cancers overexpressing miR-17-92. Oncogene 2007;26:6099–105.
9. Osada H, Tomida S, Yatabe Y, Tatematsu Y, Takeuchi T, Murakami H, et al. Roles of achaete-scute homologue 1 in DKK1 and E-cadherin repression and neuroendocrine differentiation in lung cancer. Cancer Res 2008;68:1647–55.
10. Osada H, Tatematsu Y, Yatabe Y, Horio Y, Takahashi T. ASH1 gene is a specific therapeutic target for lung cancers with neuroendocrine features. Cancer Res 2005;65:10680–5.
11. Dutta KK, Zhong Y, Liu YT, Yamada T, Akatsuka S, Hu Q, et al. Association of microRNA-34a overexpression with proliferation is cell type-dependent. Cancer Sci 2007;98:1845–52.
12. Linnoila RI. Functional facets of the pulmonary neuroendocrine system. Lab Invest 2006;86:425–44.
13. Keller DM, McWeeney S, Arsenlis A, Drouin J, Wright CV, Wang H, et al. Characterization of pancreatic transcription factor Pdx-1 binding sites using promoter microarray and serial analysis of chromatin occupancy. J Biol Chem 2007;282:32084–92.
14. Kapsimali M, Kloosterman WP, de Bruijn E, Rosa F, Plasterk RH, Wilson SW. MicroRNAs show a wide diversity of expression profiles in the developing and mature central nervous system. Genome Biol 2007;8:R173.
15. Poy MN, Hausser J, Trajkovski M, Braun M, Collins S, Rorsman P, et al. miR-375 maintains normal pancreatic alpha- and beta-cell mass. Proc Natl Acad Sci U S A 2009;106:5813–8.
16. Baroukh NN, Van Obberghen E. Function of microRNA-375 and microRNA-124a in pancreas and brain. FEBS J 2009;276: 6509–21.
17. Avnit-Sagi T, Kantorovich L, Kredo-Russo S, Hornstein E, Walker MD. The promoter of the pri-miR-375 gene directs expression selectively to the endocrine pancreas. PLoS One 2009;4:e5033.
18. Mathe EA, Nguyen GH, Bowman ED, Zhao Y, Budhu A, Schetter AJ, et al. MicroRNA expression in squamous cell carcinoma and

Downloaded from cancerres.aacrjournals.org on February 26, 2012
Copyright © 2011 American Association for Cancer Research

Published OnlineFirst August 19, 2011; DOI:10.1158/0008-5472.CAN-11-1020

adenocarcinoma of the esophagus: associations with survival. Clin Cancer Res 2009;15:6192–200.

19. Tsukamoto Y, Nakada C, Noguchi T, Tanigawa M, Nguyen LT, Uchida T, et al. MicroRNA-375 is downregulated in gastric carcinomas and regulates cell survival by targeting PDK1 and 14-3-3zeta. Cancer Res 2010;70:2339–49.

20. Liu AM, Poon RT, Luk JM. MicroRNA-375 targets Hippo-signaling effector YAP in liver cancer and inhibits tumor properties. Biochem Biophys Res Commun 2010;394:623–7.

21. Abdelmohsen K, Hutchison ER, Lee EK, Kuwano Y, Kim MM, Masuda K, et al. miR-375 inhibits differentiation of neurites by lowering HuD levels. Mol Cell Biol 2010;30:4197–210.

22. Ding L, Xu Y, Zhang W, Deng Y, Si M, Du Y, et al. MiR-375 frequently downregulated in gastric cancer inhibits cell proliferation by targeting JAK2. Cell Res 2010;20:784–93.

23. de Souza Rocha Simonini P, Breiling A, Gupta N, Malekpour M, Youns M, Omranipour R, et al. Epigenetically deregulated microRNA-375 is involved in a positive feedback loop with estrogen receptor alpha in breast cancer cells. Cancer Res 2010;70:9175–84.

24. Wang K, Degerny C, Xu M, Yang XJ. YAP, TAZ, and Yorkie: a conserved family of signal-responsive transcriptional coregulators in animal development and human disease. Biochem Cell Biol 2009; 87:77–91.

25. Bertini E, Oka T, Sudol M, Strano S, Blandino G. YAP: at the crossroad between transformation and tumor suppression. Cell Cycle 2009;8: 49–57.

26. Zhao B, Li L, Lei Q, Guan KL. The Hippo-YAP pathway in organ size control and tumorigenesis: an updated version. Genes Dev 2010;24: 862–74.

27. Strano S, Munarriz E, Rossi M, Castagnoli L, Shaul Y, Sacchi A, et al. Physical interaction with Yes-associated protein enhances p73 transcriptional activity. J Biol Chem 2001;276:15164–73.

28. Oka T, Mazack V, Sudol M. Mst2 and Lats kinases regulate apoptotic function of Yes kinase-associated protein (YAP). J Biol Chem 2008;283:27534–46.

29. Oka T, Sudol M. Nuclear localization and pro-apoptotic signaling of YAP2 require intact PDZ-binding motif. Genes Cells 2009;14: 607–15.

30. Ehsanian R, Brown M, Lu H, Yang XP, Pattatheyil A, Yan B, et al. YAP dysregulation by phosphorylation or DeltaNp63-mediated gene repression promotes proliferation, survival and migration in head and neck cancer subsets. Oncogene 2010;29:6160–71.

31. Lapi E, Di Agostino S, Donzelli S, Gal H, Domany E, Rechavi G, et al. PML, YAP, and p73 are components of a proapoptotic autoregulatory feedback loop. Mol Cell 2008;32:803–14.

32. Yuan M, Tomlinson V, Lara R, Holliday D, Chelala C, Harada T, et al. Yes-associated protein (YAP) functions as a tumor suppressor in breast. Cell Death Differ 2008;15:1752–9.

33. Zhang H, Pasolli HA, Fuchs E. Yes-associated protein (YAP) transcriptional coactivator functions in balancing growth and differentiation in skin. Proc Natl Acad Sci U S A 2011;108: 2270–5.

Downloaded from cancerres.aacrjournals.org on February 26, 2012
Copyright © 2011 American Association for Cancer Research

MOLECULAR CARCINOGENESIS 50:301–309 (2011)

Proteasomal Non-catalytic Subunit PSMD2 as a Potential Therapeutic Target in Association With Various Clinicopathologic Features in Lung Adenocarcinomas

Yasushi Matsuyama,[1,2] Motoshi Suzuki,[1] Chinatsu Arima,[1] Qin Miao Huang,[1] Shuta Tomida,[1] Toshiyuki Takeuchi,[1] Ryoji Sugiyama,[1] Yasutomo Itoh,[3] Yasushi Yatabe,[4] Hidemi Goto,[2] and Takashi Takahashi[1]*

[1]*Division of Molecular Carcinogenesis, Center for Neurological Diseases and Cancer, Nagoya University Graduate School of Medicine, Nagoya, Japan*
[2]*Department of Gastroenterology, Nagoya University Graduate School of Medicine, Nagoya, Japan*
[3]*Division of Medical Research Engineering, Nagoya University Graduate School of Medicine, Nagoya, Japan*
[4]*Department of Pathology and Molecular Diagnosis, Aichi Cancer Center, Nagoya, Japan*

We previously identified *PSMD2*, a subunit of the 19S regulatory complex of proteasomes, as a constituent of a signature associated with the acquisition of metastatic phenotype and poor prognosis in lung cancers. In the present study, we found that knockdown of *PSMD2* decreased proteasome activity, and induced growth inhibition and apoptosis in lung cancer cell lines. These effects of siRNA-mediated *PSMD2* inhibition were associated with changes in the balance between phosphorylated AKT and p38, as well as with induction of p21. In addition, patients with higher *PSMD2* expression had poorer prognosis and a small fraction of lung cancer specimens carried increased copies of *PSMD2*. Notably, our findings clearly illustrate that lung adenocarcinomas can be divided into two groups; those with and without general upregulation of proteasome pathway genes including *PSMD2*. This general upregulation was significantly more prevalent in the non-terminal respiratory unit (non-TRU)-type, a recently proposed genetically and clinicopathologically relevant expression profile-defined classification of adenocarcinomas ($P < 0.001$ by Fisher's exact test). Patients with adenocarcinomas with general upregulation had significantly shorter survival after potentially curative resection ($P = 0.0001$ by log-rank test) independent of disease stage, as shown by multivariate Cox regression analysis. Our results suggest that *PSMD2* may be a good molecular target candidate and that other co-regulated proteasome pathway genes and/or their common regulator(s) might also be potential targets, warranting future study including elucidation of the underlying common regulatory mechanism. © 2011 Wiley-Liss, Inc.

Key words: lung cancer; apoptosis; gene expression profile

INTRODUCTION

Lung cancer is the leading cause of cancer-related death in Japan, as well as in many other economically well-developed countries [1]. A better understanding of the molecular pathogenesis of this disease is thus urgently required for preventive or therapeutic breakthroughs to drastically reduce the unacceptable number of deaths. Non-small cell lung cancers (NSCLCs) are mainly comprised of adenocarcinomas, squamous cell carcinomas, and large cell carcinomas, of which adenocarcinomas are known to exhibit the highest degree of morphologic and clinical diversities.

Proteasomes are crucially involved in the execution of a number of cellular functions, such as apoptosis and cell-cycle progression in both normal and malignant cells. The 26S proteasome is an abundant multi-enzyme complex that provides the main pathway for degradation of intracellular proteins in eukaryotic cells [2]. It is found in the cytoplasm and nucleus, and consists of a 20S core catalytic cylindrical complex capped at both ends by a 19S regulatory complex [3,4]. The 20S core catalytic complex harbors the proteolytically active β1 (caspase-like), β2 (trypsin-like), and β5 (chymotrypsin-like) subunits. Despite the premise that it would be difficult to use as a target for chemotherapy while maintaining a tolerable therapeutic index,

Additional Supporting Information may be found in the online version of this article.

Abbreviations: NSCLC, non-small cell lung cancer; siRNA, small interfering RNA; TUNEL, Terminal Transferase dUTP Nick End Labeling; TRU, terminal respiratory unit.

*Correspondence to: Division of Molecular Carcinogenesis, Center for Neurological Disease and Cancer, Nagoya University Graduate School of Medicine, Nagoya 466-8550, Japan.

Received 12 August 2009; Revised 1 February 2010; Accepted 12 February 2010

DOI 10.1002/mc.20632

Published online in Wiley Online Library (wileyonlinelibrary.com).

© 2011 WILEY-LISS, INC.

many types of actively proliferating malignant cells are more sensitive to proteasome blockade than non-cancerous cells. The β5 subunit in the 20S proteasome complex is the specific target of bortezomib, the first proteasome inhibitor to enter clinical development for treatment of multiple myelomas and other malignant disorders, including lung cancers [5–7]. The present study was initiated based on our previous finding that *PSMD2*, a subunit of the 19S regulatory complex, constituted an expression signature that was associated with the acquisition of a metastatic phenotype in the NCI-H460-LNM35 lung cancer cell line as well as with poor prognosis in surgically operated lung cancer patients [8]. Herein, we present evidence of apoptosis by small interfering RNA (siRNA)-mediated inhibition of *PSMD2* in lung cancer cell lines and the presence of increased copies of the *PSMD2* gene in a fraction of lung cancer tissue specimens. In addition, we report that not only *PSMD2*, but also multiple genes of the 26S proteasome and those involved in their assembly were co-upregulated, showing a significant association with shorter survival in surgically treated adenocarcinoma patients.

MATERIALS AND METHODS

Cell Lines

We used ACC-LC-94, ACC-LC-319, A549, and A427 cells derived from human lung adenocarcinoma cell lines, as well as Calu1 cells from a human lung squamous cell carcinoma cell line. NCI-H460-LNM35 cells [9] (hereafter termed LNM35), a highly metastatic subline of the NCI-H460 human lung large cell carcinoma cell line, were also used. Culture conditions and derivations of the panel of lung cancer cell lines were as described previously [10]. Human dermal fibroblasts, TIG112 cells, were also utilized and cultured in Dulbecco's Modified Eagle Medium (DMEM) with 20% fetal calf serum [11].

Antibodies and siRNAs

The following antibodies were used for Western blot analysis: anti-PSMD2 (ABR PA1-964) and anti-β-actin (Sigma–Aldrich, St. Louis, MO); anti-lamin B, anti-cyclin A, and anti-cyclinB1 (Santa Cruz Biotechnology, Santa Cruz, CA); anti-caspase-7, anti-p53, anti-phospho-p38 MAPK (Thr180/Tyr182), anti-phospho-AKT (Ser473), anti p53, and anti-AKT (Cell Signaling Technology, Danvers, MA); and anti-BCL2, anti-BAD, anti-p38α, and anti-p21 (BD Transduction Laboratories, San Jose, CA). The sequences of siRNA against *PSMD2* (si*PSMD2*) used were as follow: sense strand, 5′-CACACUAUGGCAAACUGAATT; and anti-sense strand, 5′-UUCAGUUUGCCAUAGUGUGTT. si*CTRL* refers to the AM4611 *Silencer*® Negative Control #1 siRNA obtained from Applied Biosystems (Foster City, CA). Silencing efficiency was evaluated by both Western blotting and TaqMan-based real-time reverse transcription-PCR analyses (TaqMan gene expression, Hs 01092070_g1, Applied Biosystems) (data not shown for the latter).

3-(4,5-Dimethylthiazol-2-yl)-2, 5-Diphenyltetrazolium Bromide (MTT) Assay

Cells were plated at a density of 8×10^4 in 0.5 mL of culture medium on six-well plates. The next day, either si*PSMD2* or si*CTRL* was transfected at a final concentration of 1 or 10 nM using RNAi MAX (Invitrogen, Carlsbad, CA) (day 0). Viable cells were measured in triplicate using TetraColor One (Seikagaku, Tokyo, Japan) in reference to the viability of non-treated cells on various days after transfection.

Proteasome Activity Assay

Proteasome activity was measured using a 20S proteasome activity assay kit (Chemicon, Temecula, CA), according to the manufacturer's instructions. In brief, control or siRNA-treated cells were lysed in a lysis buffer [150 mM NaCl, 20 mM Tris–HCl (pH 7.2), 1% Triton X-100, 1 mM DTT] without protease inhibitors. Total cell lysates (1.6 μg) prepared from LNM35 cells treated with either si*PSMD2* or si*CTRL* were incubated with 20 μmol/L of the fluorogenic substrate Suc-Leu-Leu-Val-Tyr-AMC for determining proteasomal chymotrypsin-like activity at 37°C in 100 μL of assay buffer [250 mM HEPES-KOH (pH 7.5), 5 mM EDTA, 0.5% NP40, and 0.01% SDS]. Free AMC liberated by the substrate hydrolysis was quantified using a microtiter plate fluorometer (ARVO™ MX 1420 multilabel counter, PerkinElmer, Kanagawa, Japan) with excitation at 355 nm and emission at 460 nm.

Terminal Transferase dUTP Nick End Labeling (TUNEL) Assay

Cells were plated at a density of 8×10^4 in 0.5 mL of culture medium on six-well plates and cultured for 24 h, then transfected with siRNA, as described above (day 0). Two days later, they were stained using an *in situ* cell death detection kit (Roche Diagnostics, Indianapolis, IN) according to the supplier's protocol.

Flow Cytometric Analysis

Cells were plated at a density of 1.5×10^5 in 4 mL of culture medium on 6-cm dishes. The next day, si*PSMD2* or si*CTRL* (10 nM) was transfected as described above. After 48 h of continuous exposure, the cells were treated with a phosphate-buffered saline solution containing 0.5% NP-40 and 50 μg/mL of propidium iodide (Sigma–Aldrich). Cellular DNA contents were measured using a FACSCalibur flow cytometer equipped with the CELLQuest program (BD Biosciences), as described previously [12].

Patients and Statistical Analysis

Our previous dataset comprising 149 patients with NSCLC, which included 90 patients with adenocar-

cinomas, was used in the present study [13] (GSE11969). Adenocarcinoma cases were divided into high and low expression groups by comparison with the median expression level of PSMD2 in the 90 adenocarcinoma specimens. Kaplan–Meier survival curves were used to estimate survival rate as a function of time and survival differences were analyzed by a log-rank test, as described previously [1314]. Approval for this study was obtained from the institutional review boards of both Nagoya University and Aichi Cancer Center.

TaqMan-based Copy Number Analysis

Gene copies of *PSMD2* and *PIK3CA* in each tumor were analyzed using TaqMan Universal PCR Master Mix (Applied Biosystems) with the following PCR primers and TaqMan probes: Hs03470293_cn and Hs04761440_cn for *PSMD2* and *PIK3CA*, respectively. Quantification of the control *ALB* has been described [15]. The fold increase in copy number in a given cancer tissue was calculated as the ratio of either *PSMD2* or *PIK3CA* signals to the *ALB* signal, followed by further normalization to that of the mean value obtained from 46 normal lung DNA samples.

RESULTS

Reduction of Lung Cancer Cell Proliferation by Inhibition of *PSMD2* Expression

First, we examined two human lung adenocarcinoma cell lines, LNM35 and ACC-LC-94, as well as a human normal fibroblast cell line, TIG112, for their response to siRNA-mediated inhibition of *PSMD2*. Western blot analysis showed a significant reduction of PSMD2 expression in all three cell lines treated with si*PSMD2* (Figure 1A). Furthermore, an MTT assay conducted on day 2 after the start of siRNA treatment revealed that si*PSMD2* treatment significantly reduced proliferation in both LNM35 and ACC-LC-94, but not in TIG112, when compared to treatment with the negative control si*CTRL* (Figure 1B). ACC-LC-94 and LNM35 showed gradual and further incremental decreases in proliferating cells over time, whereas TIG112 did not (Figure 1C).

Inhibition of Proteasome Activity in Cells Treated with siRNA Against *PSMD2*

PSMD2 is an ortholog of the proteasome subunit of *Rpn1/NAS1* in *Saccharomyces cerevisiae* as well as *Mts4* in *Schizosaccharomyces pombe* [16,17]. We examined the proteolytic cleavage activity of PSMD2 using a fluorogenic peptide as a substrate for various times to confirm that PSMD2 functions as a proteasome subunit in human lung cancer cells. Cell lysates were prepared from LNM35 cells that had been treated with either si*PSMD2* or si*RNA* for 48 h, and subjected to proteasome activity analysis. si*PSMD2* treatment clearly suppressed the proteasome activity (Figure 2),

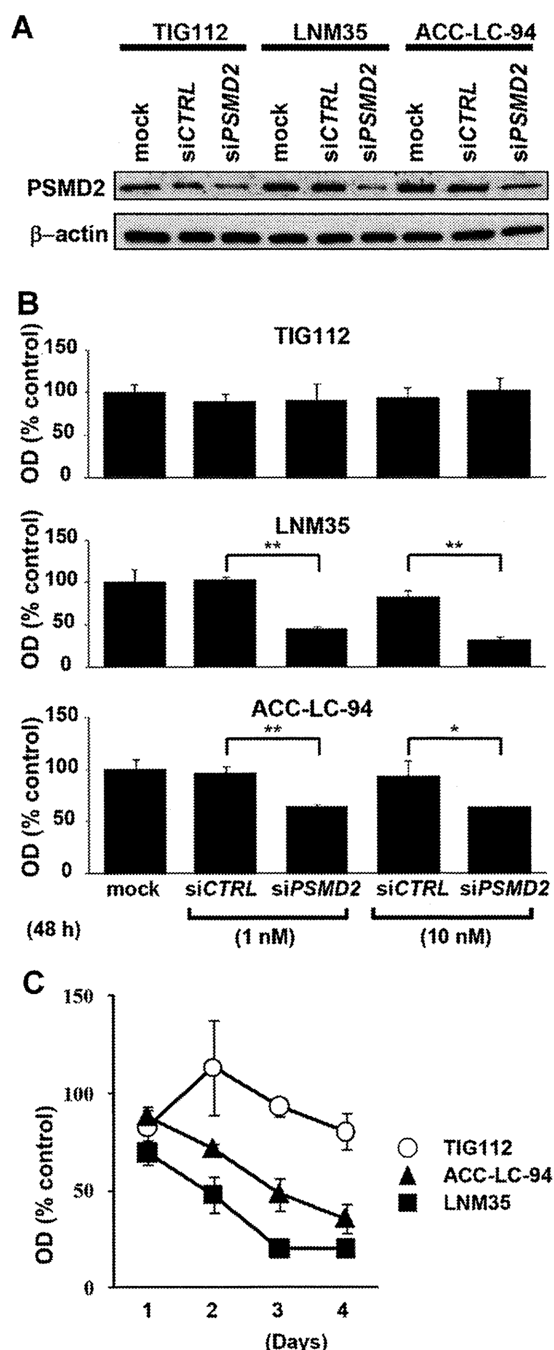

Figure 1. Reduction of cell growth by *PSMD2* knockdown in lung cancer cell lines (LNM35 and ACC-LC-94), but not in a normal fibroblast cell line (TIG112). (A) Western blot analysis of PSMD2 at 48 h after siRNA treatment. β-actin was used as a loading control. (B) MTT assay of cells treated with either 1 or 10 nM siRNA for 48 h. * and ** indicate the significant growth suppression with the *P* values of $P<0.05$ and $P<0.01$, respectively. (C) Results of MTT assay that measured cell growth for up to 4 days after treatment with 10 nM siRNA. OD values with si*CTRL* in (B) and (C) were regarded as 100%. si*PSMD2*, siRNA against *PSMD2*; si*CNTL*, negative control siRNA.

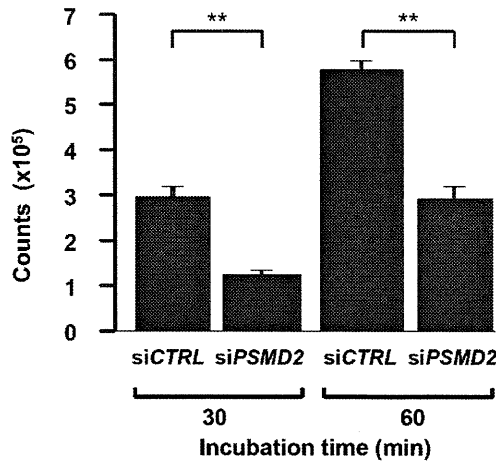

Figure 2. Reduction of proteasome activity by *PSMD2* knockdown. Intracellular proteasome activity was measured using cell lysates of LNM35 treated with either 10 nM si*CTRL* or si*PSMD2* for 2 days. Data shown were obtained after incubation for 30 and 60 min, during which linear increases in proteasome activity were observed. **Indicates the significant reduction in proteasome activity with $P < 0.01$.

showing that *PSMD2* is required for 26S proteasome functions in human lung cancer cells.

Growth Inhibitory Effects of *PSMD2* Knockdown in Panel of Lung Adenocarcinoma Cell Lines

A panel of human lung adenocarcinoma specimens was examined for growth inhibition in response to *PSMD2* knockdown using an MTT assay. Western blot analysis showed apparent reduction of PSMD2 expression in all cell lines treated with si*PSMD2* (Figure 3A). An MTT assay was performed on day 2 after initiating siRNA treatment, which showed significantly reduced proliferation in LNM35, ACC-LC-94, ACC-LC-319, and A549 (Figure 3B). In contrast, growth inhibition was not observed in A427, Calu1, or TIG112.

Induction of Apoptosis by *PSMD2* Knockdown in Lung Cancer Cell Lines

Next, we performed TUNEL and flow cytometric assays to determine whether *PSMD2* knockdown induced apoptosis. The TUNEL assay results clearly showed induction of apoptosis by si*PSMD2* treatment in LNM35, but not in TIG112 (Figure 4A). The results of flow cytometric analysis also indicated apoptosis occurrence in LNM35 cells treated with si*PSMD2*, with a significant increase in the subG1 fraction (Figure 4B). The induction of apoptosis in si*PSMD2*-treated LNM35 cells was further substantiated by Western blot analysis, which detected cleaved forms of an effector caspase, caspase-7, and lamin B, indicating activation of the apoptotic pathway (Figure 4C). Furthermore, we found that a phosphorylated form of p38 was increased as was a phosphorylated form of AKT (Figure 4D), indicating

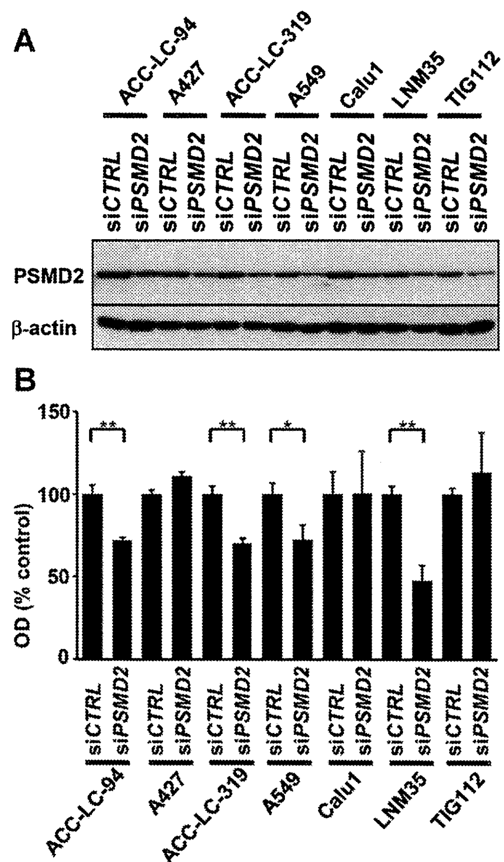

Figure 3. Reduction of cell growth by *PSMD2* knockdown in panel of lung cancer cell lines. (A) Western blot analysis of PSMD2 in cells treated with 10 nM siRNA for 48 h. β-actin was used as a loading control. (B) Results of MTT assay showing varying degrees of cell growth inhibition by si*PSMD2* treatment. OD values with si*CTRL* were regarded as 100%. * and ** indicate the significant growth suppression with the *P* values of $P < 0.05$ and $P < 0.01$, respectively.

that PSMD2 inhibition affects the crucial balance between active forms of a pro-apoptotic MAPK, p38, and a survival kinase, AKT [18,19]. We also observed an increase in G1 in si*PSMD2*-treated LNM35 cells (Figure 4E), which appeared to be consistent with marked induction of p21, a negative regulator of cell cycle and known target for proteasomes (Figure 4D). In contrast, we did not observe any effects of si*PSMD2* treatment in LNM35 cells on the expression of BCL2, BCL-x, Bad, cyclin A, or cyclin B, whereas p53 was modestly affected by si*PSMD2* treatment (Supplementary Figure 1), consistent with a previous report that p53 is degraded in a PSMD2/S2 dependent manner [20].

Increased Gene Copies of *PSMD2* and Relationship of *PSMD2* Expression with Postoperative Survival in Lung Adenocarcinomas

The present findings that *PSMD2* expression was involved in lung adenocarcinoma cell growth prompted us to analyze the relationship between the

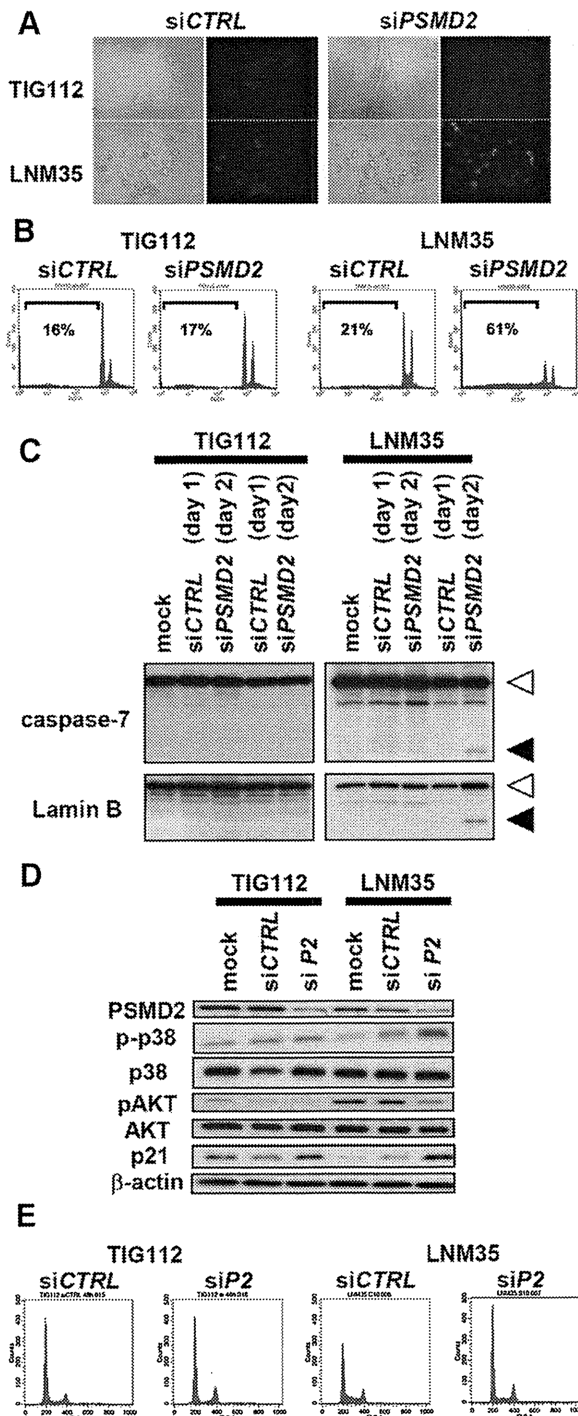

Figure 4. Apoptosis induction and G1 phase accumulation in cells treated with si*PSMD2*. (A) TUNEL assay results showing apoptosis induction in cells treated with siRNA for 48 h. (B) Flow cytometric analysis showing increased subG1 fraction in LNM35 treated with si*PSMD2*. (C) Western blot analysis of proteolytic cleavage of caspase 7 and lamin B in cells treated with siRNAs for the indicated periods. Closed and open arrowheads indicate cleaved and intact forms, respectively. (D) Western blot analysis of various apoptosis- and cell cycle-related proteins in cells after 48 h of siRNA treatment. (E) Flow cytometric analysis of cell cycle progression in cells after 48 h of siRNA treatment.

level of *PSMD2* expression and postoperative survival in surgically treated adenocarcinoma patients using our previously published dataset obtained by microarray analysis. Kaplan–Meier survival curves generated according to expression of *PSMD2* either higher or lower than the median value in the 90 adenocarcinomas revealed poorer prognosis in patients with higher expression ($P = 0.047$ by log-rank test; Figure 5A).

Several studies have shown that genetic mutations that directly activate the PI3K signaling pathway are common in human cancers. Beside the loss of the tumor suppressor PTEN, somatic activating mutations and amplification of *PIK3CA* and *AKT* are occasionally observed in epithelial cancers [21]. Among the PI3K signaling genes, *PIK3CA* resides at 3q26.3, which is close to *PSMD2* at 3q27.1, and locates in the area where gains uniquely related to lung cancer at 3q24–q29 [22–24]. For this reason, we investigated the relationship between the expression levels of *PSMD2* and *PIK3CA*. Interestingly, we found that the *PSMD2* expression was significantly associated with that of *PIK3CA* in the 90 adenocarcinoma cases (Figure 5B). Next, we examined 220 NSCLC cases including 148 with adenocarcinomas for the presence of increased gene copies of *PSMD2* and *PIK3CA* using a TaqMan-based PCR analysis. Our results showed that 12 cases (5.5%) carried more than a 2.5-fold gain at the *PSMD2* locus, while 9 (4.1%) had similar levels of gain at the *PIK3CA* locus (Figure 5C). Modest gains between 1.5- and 2.5-fold for both *PSMD2* and *PIK3CA* were also observed in 38 (17.3%) and 15 (6.8%) cases, respectively. Notably, a single case exhibited 4.7-fold increase only at the *PSMD2* locus without any appreciable increase at *PIK3CA*.

Identification of Co-regulated Expression of Proteasome Pathway Genes, and Association With Expression Profile-defined Subtype and Prognosis in Lung Adenocarcinomas

It is possible that general co-upregulation of proteasome pathway genes is advantageous for cancer development and associated with clinicopathologic features such as postoperative survival. Therefore, we selected a gene set comprised of various 19S and 20S subunits of the 26S proteasome, as well as those functioning in proteasome assembly [25], and performed an unsupervised hierarchical clustering analysis of the 90 adenocarcinoma cases (Figure 6A). We found that the cases could be clearly divided into two groups; those with and without a general high expression of genes involved in proteasome-mediated protein degradation. Cluster 1, consisting of cases with general high expression, showed a significant association with adenocarcinomas with non-terminal respiratory unit (non-TRU)-type histology ($P < 0.001$ by Fisher's exact test), a recently proposed expression Profile-defined subtype, as well as a lack of bronchiole alveolar features ($P = 0.005$;

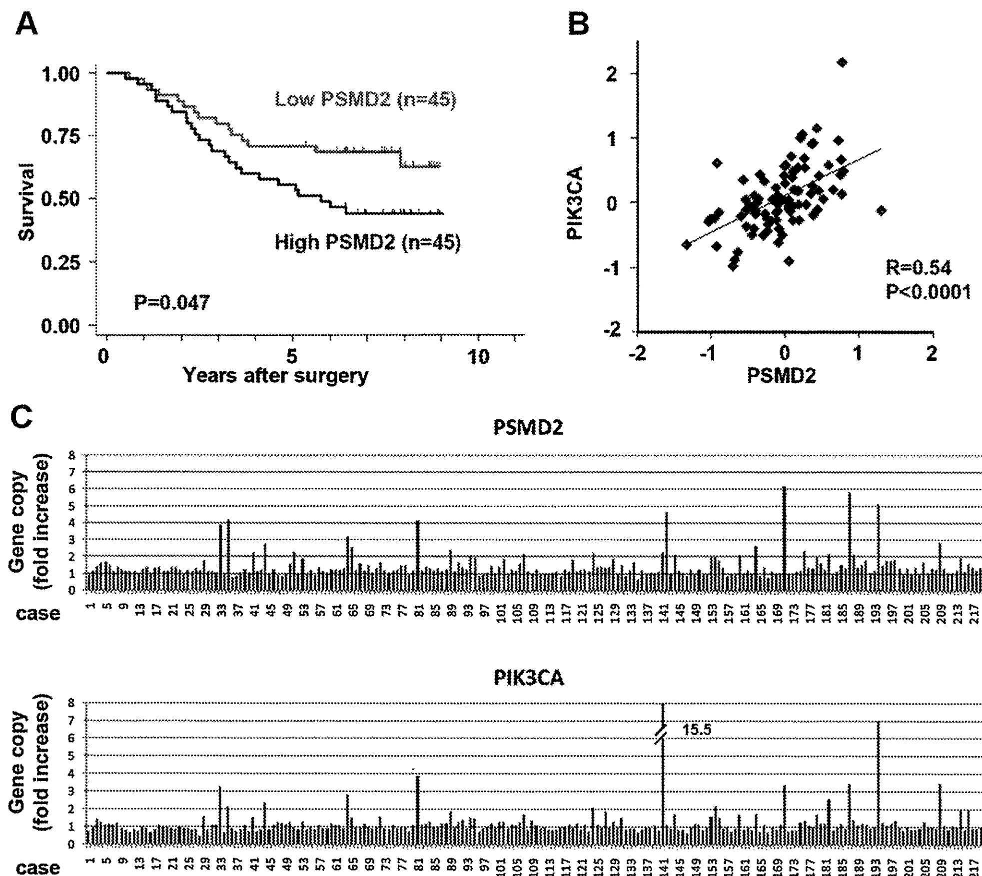

Figure 5. Relationship between *PSMD2* expression and postoperative survival in patients following potentially curative resection. (A) Kaplan–Meier survival curves according to expression levels of *PSMD2* in 90 adenocarcinoma cases [13]. The cases were divided into high and low expression groups based on the median value of *PSMD2* expression. (B) Scatter plot analysis showing a positive correlation between expression levels of *PSMD2* and *PIK3CA* ($R = 0.54$, $P < 0.0001$). (C) TaqMan-based gene dosage analysis of PSMD2 and PIK3CA showing modest increases in a small fraction of NSCLC tissues. ALB signals were used as an internal control for loading. The mean value obtained from 48 normal lung tissues was set as 1.

Table 1). In addition, we observed significant associations of cluster 1 with past smoking history ($P = 0.020$) and higher histological grade ($P = 0.031$). Kaplan–Meier survival curves revealed that patients with adenocarcinomas belonging to cluster 1 had a significantly shorter survival than that of those in cluster 2 ($P = 0.0001$ by log-rank test; Figure 6B). Multivariate Cox regression analysis also showed that cluster distinction based on the proteasome-mediated protein degradation pathway was a significant predictor of postoperative prognosis (Hazard ratio = 3.372; $P = 0.001$), independent of p-Stage (Hazard ratio = 3.135; $P = 0.001$; Table 2).

DISCUSSION

It has been suggested that PSMD2 is a functional equivalent to yeast proteins of RPN1/NAS1 in *S. cerevisiae* and Mts4 in *S. pombe*, based on findings that enforced expression of *PSMD2* suppressed growth defects in both *rpn1/nas1* and *mts4* disrupted yeast cells [16,17]. In the 19S regulatory complex, RPN1/NAS1 is a component of the base complex, which is required for substrate translocation and gating of the proteolytic channel, and possibly serves as a docking site for a substrate-recruitment factor in the 19S complex [26]. In the present study, we found that siRNA-mediated inhibition of *PSMD2* in human lung cancer cells resulted in a reduction of proteasome activity, in association with induction of apoptosis and increase in number of cells in the G1 phase. A decrease in phosphorylated AKT and increase in phosphorylated p38 in si*PSMD2*-treated cells, as well as induction of p21 appears to be consistent with the treatment effects. A future study to elucidate how such molecular consequences are mediated in *PSMD2*-inhibited lung cancer cells is warranted.

Interestingly, *PSMD2* has been reported to constitute cancer-associated signatures including those related to undifferentiated cancers, metastatic phenotypes, and prognosis in breast cancer [8,27–29]. Those previous studies identified either *PSMD2* alone, or *PSMD2* and *PSMD7* among various

A

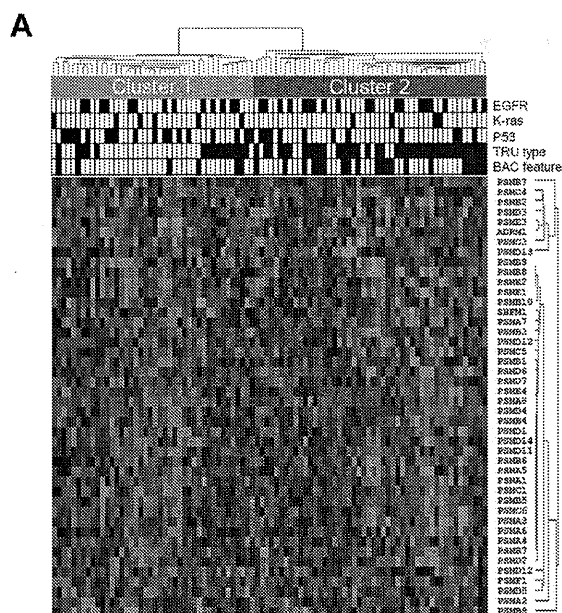

B

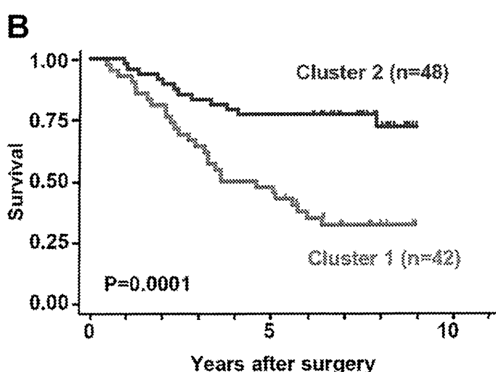

Figure 6. Relationships among expressions of proteasome pathway genes and various clinicopathologic features. (A) Hierarchical clustering analysis of 90 adenocarcinoma cases showing co-upregulation of a majority of the proteasome pathway genes. (B) Kaplan–Meier survival curves according to the two major clusters in (A) showing a significant difference in postoperative survival ($P = 0.0001$ by log-rank test).

Table 1. Associations Among Two Major Clusters and Clinicopathologic Features

Variables	Cluster 1	Cluster 2	*P*-Value*
Age (yr)			
>61	18	22	0.834
≤61	24	26	
Sex			
Male	26	21	0.096
Female	16	27	
Smoking status			
Current/former	27	18	0.020
Never	15	30	
Histologic grade			
Poor/moderate	21	13	0.031
Well	21	35	
p-Stage			
II or III	20	18	0.395
I	22	30	
EGFR			
Mutant	13	19	0.509
Wild-type	29	29	
K-ras			
Mutant	6	4	0.505
Wild-type	36	44	
p53			
Mutant	18	11	0.070
Wild-type	24	37	
EP-defined subtype[a]			
TRU	15	38	<0.001
Non-TRU	27	10	
BAC features			
+	6	20	0.005
−	36	28	

*Fisher's exact test.
[a]EP-defined subtype, expression profile-defined subtype of adenocarcinomas (13).

members of the *PSMD* family. In addition, Wan et al. [30] conducted a large-scale screening study and reported that introduction of *PSMD2* caused stimulated colony formation of NIH3T3 cells by more than six-fold, suggesting that *PSMD2* offers a growth advantage to cells under certain conditions. In the present study, though *PSMD2* and *PIK3CA* expressions were significantly correlated and often had the same increased gene copies, there was an exception of lung cancer specimen with increased gene copies only at the *PSMD2* locus, suggesting that *PSMD2* may not be a mere bystander of *PIK3CA*, a well established cancer associated gene.

Our results clearly demonstrated that genes encoding components of the 26S proteasome and those involved in proteasome assembly are co-regulated in lung adenocarcinomas, showing a significant association between general high expression of the proteasome pathway genes and shorter postoperative survival. These suggest that such co-regulated upregulation may confer greater advantage to cancer cell growth during cancer development. Further, they indicated the possibility of a common transcriptional regulatory mechanism(s) among the proteasome-related genes, which may be an effective target(s) for diminishing proteasome activity for cancer treatment.

It is also interesting to note that a general high expression of proteasome-related genes was highly significantly associated with the non-TRU type of adenocarcinomas. We previously proposed a TRU/non-TRU classification as a genetically and clinically relevant grouping of adenocarcinoma patients [31,32], which was further substantiated by a report of their marked distinctions in expression profiles [13]. Similar observations were subsequently reported by other groups, confirming the existence of adenocarcinoma subtypes with distinct expression profiles similarly associated with various

Table 2. Results of Multivariate Cox Regression Analysis

Variables	Unfavorable/favorable	Hazard ratio	95% CI*	P-Value
Age (yr)	>61/≤61	1.158	0.565–2.373	0.689
Sex	Male/female	0.960	0.406–2.273	0.926
Smoking status	Current or former/never	0.660	0.252–1.732	0.399
Histologic grade	Poor or moderate/well	1.830	0.898–3.727	0.096
p-Stage	II or III/I	3.135	1.591–6.177	0.001
EP-defined subtype[a]	Non-TRU/TRU	1.376	0.637–2.973	0.416
Cluster	Cluster 1/cluster 2	3.372	1.643–6.921	0.001

*95% CI, 95% confidence interval.
EP-defined subtype, expression profile-defined subtype of adenocarcinomas (13).

clinicopathologic features [33–35]. Following our previous report of a significant association of TRU-type with EGFR mutations [13,31], the present findings add another layer of molecular distinctions to the TRU/non-TRU classification of adenocarcinomas, that is, prevalent high expression of proteasome pathway genes specifically in the non-TRU type, which suggests that proteasome inhibitors may be more effective for this adenocarcinoma subtype.

Taken together, the present study results show that PSMD2 may be a good candidate for development of novel therapy for lung cancer treatment. In addition, the findings of our expression profile analysis indicate that other co-regulated proteasome pathway genes and/or common regulator(s) of their expression may be relevant potential target(s).

ACKNOWLEDGMENTS

This work was supported in part by a Grant-in-Aid for Scientific Research on Priority Areas from the Ministry of Education, Culture, Sports, Science, and Technology of Japan, a Grant-in-Aid for Scientific Research from the Japan Society for the Promotion of Science (C), and a grant from the Novartis Foundation (Japan) for the Promotion of Science.

REFERENCES

1. Osada H, Takahashi T. Genetic alterations of multiple tumor suppressors and oncogenes in the carcinogenesis and progression of lung cancer. Oncogene 2002;21:7421–7434.
2. Adams J. The proteasome: A suitable antineoplastic target. Nat Rev Cancer 2004;4:349–360.
3. Peters JM, Cejka Z, Harris JR, Kleinschmidt JA, Baumeister W. Structural features of the 26 S proteasome complex. J Mol Biol 1993;234:932–937.
4. Brooks P, Fuertes G, Murray RZ, et al. Subcellular localization of proteasomes and their regulatory complexes in mammalian cells. Biochem J 2000;346:155–161.
5. Davies AM, Lara PN, Jr., Mack PC, Gandara DR. Incorporating bortezomib into the treatment of lung cancer. Clin Cancer Res 2007;13:s4647–s4651.
6. Orlowski RZ, Stinchcombe TE, Mitchell BS, et al. Phase I trial of the proteasome inhibitor PS-341 in patients with refractory hematologic malignancies. J Clin Oncol 2002;20:4420–4427.
7. Richardson PG, Barlogie B, Berenson J, et al. A phase 2 study of bortezomib in relapsed, refractory myeloma. N Engl J Med 2003;348:2609–2617.
8. Tomida S, Yanagisawa K, Koshikawa K, et al. Identification of a metastasis signature and the DLX4 homeobox protein as a regulator of metastasis by combined transcriptome approach. Oncogene 2007;26:4600–4608.
9. Kozaki K, Miyaishi O, Tsukamoto T, et al. Establishment and characterization of a human lung cancer cell line NCI-H460-LNM35 with consistent lymphogenous metastasis via both subcutaneous and orthotopic propagation. Cancer Res 2000;60:2535–2540.
10. Nakagawa T, Hayashita Y, Maeno K, et al. Identification of decatenation G2 checkpoint impairment independently of DNA damage G2 checkpoint in human lung cancer cell lines. Cancer Res 2004;64:4826–4832.
11. Tokumaru S, Suzuki M, Yamada H, Nagino M, Takahashi T. let-7 regulates Dicer expression and constitutes a negative feedback loop. Carcinogenesis 2008;29:2073–2077.
12. Matsubara H, Takeuchi T, Nishikawa E, et al. Apoptosis induction by antisense oligonucleotides against miR-17-5p and miR-20a in lung cancers overexpressing miR-17-92. Oncogene 2007;26:6099–6105.
13. Takeuchi T, Tomida S, Yatabe Y, et al. Expression profile-defined classification of lung adenocarcinoma shows close relationship with underlying major genetic changes and clinicopathologic behaviors. J Clin Oncol 2006;24:1679–1688.
14. Tomida S, Takeuchi T, Shimada Y, et al. Relapse-related molecular signature in lung adenocarcinomas identifies patients with dismal prognosis. J Clin Oncol 2009;27:2793–2799.
15. Tanaka H, Yanagisawa K, Shinjo K, et al. Lineage-specific dependency of lung adenocarcinomas on the lung development regulator TTF-1. Cancer Res 2007;67:6007–6011.
16. Tsurumi C, Shimizu Y, Saeki M, et al. cDNA cloning and functional analysis of the p97 subunit of the 26S proteasome, a polypeptide identical to the type-1 tumor-necrosis-factor-receptor-associated protein-2/55.11. Eur J Biochem 1996;239:912–921.
17. Wilkinson CR, Wallace M, Seeger M, Dubiel W, Gordon C. Mts4, a non-ATPase subunit of the 26 S protease in fission yeast is essential for mitosis and interacts directly with the ATPase subunit Mts2. J Biol Chem 1997;272:25768–25777.
18. Wagner EF, Nebreda AR. Signal integration by JNK and p38 MAPK pathways in cancer development. Nat Rev Cancer 2009;9:537–549.
19. Lowe SW, Cepero E, Evan G. Intrinsic tumour suppression. Nature 2004;432:307–315.
20. Zhang X, Turnell AS, Gorbea C, Mymryk JS, Gallimore PH, Grand RJ. The targeting of the proteasomal regulatory subunit S2 by adenovirus E1A causes inhibition

of proteasomal activity and increased p53 expression. J Biol Chem 2004;279:25122–25133.

21. Engelman JA, Luo J, Cantley LC. The evolution of phosphatidylinositol 3-kinases as regulators of growth and metabolism. Nat Rev Genet 2006;7:606–619.
22. Lo KC, Stein LC, Panzarella JA, Cowell JK, Hawthorn L. Identification of genes involved in squamous cell carcinoma of the lung using synchronized data from DNA copy number and transcript expression profiling analysis. Lung Cancer 2008;59:315–331.
23. Pei J, Balsara BR, Li W, et al. Genomic imbalances in human lung adenocarcinomas and squamous cell carcinomas. Genes Chromosomes Cancer 2001;31:282–287.
24. Petersen I, Bujard M, Petersen S, et al. Patterns of chromosomal imbalances in adenocarcinoma and squamous cell carcinoma of the lung. Cancer Res 1997;57:2331–2335.
25. Tanaka K. The proteasome: Overview of structure and functions. Proc Jpn Acad Ser B Phys Biol Sci 2009;85:12–36.
26. Elsasser S, Gali RR, Schwickart M, et al. Proteasome subunit Rpn1 binds ubiquitin-like protein domains. Nat Cell Biol 2002;4:725–730.
27. Naderi A, Teschendorff AE, Barbosa-Morais NL, et al. A gene-expression signature to predict survival in breast cancer across independent data sets. Oncogene 2007;26:1507–1516.
28. Rhodes DR, Yu J, Shanker K, et al. Large-scale meta-analysis of cancer microarray data identifies common transcriptional profiles of neoplastic transformation and progression. Proc Natl Acad Sci USA 2004;101:9309–9314.
29. van 't Veer LJ, Dai H, van de Vijver MJ, et al. Gene expression profiling predicts clinical outcome of breast cancer. Nature 2002;415:530–536.
30. Wan D, Gong Y, Qin W, et al. Large-scale cDNA transfection screening for genes related to cancer development and progression. Proc Natl Acad Sci USA 2004;101:15724–15729.
31. Yatabe Y, Kosaka T, Takahashi T, Mitsudomi T. EGFR mutation is specific for terminal respiratory unit type adenocarcinoma. Am J Surg Pathol 2005;29:633–639.
32. Yatabe Y, Mitsudomi T, Takahashi T. TTF-1 expression in pulmonary adenocarcinomas. Am J Surg Pathol 2002;26: 767–773.
33. Shibata T, Hanada S, Kokubu A, et al. Gene expression profiling of epidermal growth factor receptor/KRAS pathway activation in lung adenocarcinoma. Cancer Res 2007;98: 985–991.
34. Hayes DN, Monti S, Parmigiani G, et al. Gene expression profiling reveals reproducible human lung adenocarcinoma subtypes in multiple independent patient cohorts. J Clin Oncol 2006;24:5079–5090.
35. Motoi N, Szoke J, Riely GJ, et al. Lung adenocarcinoma: Modification of the 2004 WHO mixed subtype to include the major histologic subtype suggests correlations between papillary and micropapillary adenocarcinoma subtypes, EGFR mutations and gene expression analysis. Am J Surg Pathol 2008;32:810–827.

A Novel Network Profiling Analysis Reveals System Changes in Epithelial-Mesenchymal Transition

Teppei Shimamura[1]*, Seiya Imoto[1], Yukako Shimada[2], Yasuyuki Hosono[2], Atsushi Niida[1], Masao Nagasaki[1], Rui Yamaguchi[1], Takashi Takahashi[2], Satoru Miyano[1]

1 Human Genome Center, Institute of Medical Science, University of Tokyo, Minato-ku, Tokyo, Japan, 2 Nagoya University Graduate School of Medicine, Showa-ku, Nagoya, Japan

Abstract

Patient-specific analysis of molecular networks is a promising strategy for making individual risk predictions and treatment decisions in cancer therapy. Although systems biology allows the gene network of a cell to be reconstructed from clinical gene expression data, traditional methods, such as Bayesian networks, only provide an averaged network for all samples. Therefore, these methods cannot reveal patient-specific differences in molecular networks during cancer progression. In this study, we developed a novel statistical method called NetworkProfiler, which infers patient-specific gene regulatory networks for a specific clinical characteristic, such as cancer progression, from gene expression data of cancer patients. We applied NetworkProfiler to microarray gene expression data from 762 cancer cell lines and extracted the system changes that were related to the epithelial-mesenchymal transition (EMT). Out of 1732 possible regulators of E-cadherin, a cell adhesion molecule that modulates the EMT, NetworkProfiler, identified 25 candidate regulators, of which about half have been experimentally verified in the literature. In addition, we used NetworkProfiler to predict EMT-dependent master regulators that enhanced cell adhesion, migration, invasion, and metastasis. In order to further evaluate the performance of NetworkProfiler, we selected Krueppel-like factor 5 (KLF5) from a list of the remaining candidate regulators of E-cadherin and conducted *in vitro* validation experiments. As a result, we found that knockdown of KLF5 by siRNA significantly decreased E-cadherin expression and induced morphological changes characteristic of EMT. In addition, *in vitro* experiments of a novel candidate EMT-related microRNA, miR-100, confirmed the involvement of miR-100 in several EMT-related aspects, which was consistent with the predictions obtained by NetworkProfiler.

Citation: Shimamura T, Imoto S, Shimada Y, Hosono Y, Niida A, et al. (2011) A Novel Network Profiling Analysis Reveals System Changes in Epithelial-Mesenchymal Transition. PLoS ONE 6(6): e20804. doi:10.1371/journal.pone.0020804

Editor: Eric J. Bernhard, National Cancer Institute, United States of America

Received November 2, 2010; **Accepted** May 13, 2011; **Published** June 7, 2011

Copyright: © 2011 Shimamura et al. This is an open-access article distributed under the terms of the Creative Commons Attribution License, which permits unrestricted use, distribution, and reproduction in any medium, provided the original author and source are credited.

Funding: This research was supported by "Research and Development of the Next-Generation Integrated Simulation of Living Matter" (a part of the Development and Use of the Next-Generation Supercomputer Project of MEXT) and "Integrative Systems Understanding of Cancer for Advanced Diagnosis, Therapy and Prevention" (Grant-in-Aid for Scientific Research on Innovative Areas from MEXT, Japan). The funders had no role in study design, data collection and analysis, decision to publish, or preparation of the manuscript.

Competing Interests: The authors have declared that no competing interests exist.

* E-mail: shima@ims.u-tokyo.ac.jp

Introduction

Currently, several large-scale omics projects, such as the National Cancer Institute's Cancer Genome Atlas (http://cancergenome.nih.gov/) and the Sanger Institute's Cancer Genome Project (http://www.sanger.ac.uk/genetics/CGP/), produce large amounts of data, including genomic, epigenomic, and transcriptomic information, about cancer patients or cell lines. Two challenges in omics are to construct and analyze patient-specific molecular networks to develop a comprehensive understanding of the molecular mechanisms of tumorigenesis and to identify molecules that are critical for tumor proliferation and progression [1]. If these challenges can be overcome, it may be possible to personalize cancer therapy, improve its efficacy, and reduce its toxicity and cost [2,3].

Systems biology integrates various types of omics data and computational tools to represent and analyze complex biological systems. For example, gene network estimation that is based on Bayesian networks or mutual information networks can reconstruct biological systems from gene expression data [4]. However, most traditional gene network estimation methods construct a static network by using gene expression data from different cellular conditions. As a result, these methods only produce an averaged network for all patients and cannot reveal patient-specific molecular mechanisms of cancer. In addition, it is very difficult to infer a patient-specific gene network from only a few gene expression profiles of the patient without making any assumptions about the network.

In this study, we developed a novel statistical method called NetworkProfiler, which infers patient-specific gene regulatory networks from a dataset of cancer gene expression profiles. NetworkProfiler is based on a statistical graphical model with varying coefficients and a kernel-based data integration method with elastic net regularization for parameter estimation. A key feature of NetworkProfiler is that the strengths of the relationships between genes are allowed to vary depending on cancer characteristics, such as cancer progression, metastasis, disease-free survival, and drug sensitivity. NetworkProfiler groups samples according to the specific cancer characteristics so that neighboring samples have common gene regulatory systems. Then, by integrating the gene expression profiles of neighboring samples with a kernel method, NetworkProfiler produces a gene regulatory network for each sample. Finally, we analyzed 2 post-analysis to discover upstream regulatory genes and downstream target genes for specific cancer characteristics. Network-

Profiler is the first algorithm for constructing patient-specific gene regulatory networks from clinical cancer gene expression data to elucidate cancer heterogeneity.

We applied NetworkProfiler to gene expression microarray data from 762 cancer cell lines to determine system changes related to the epithelial-mesenchymal transition (EMT). The epithelial-mesenchymal transition (EMT) is a process that changes proliferating cells from an aplanetic state to a motile state [5], which allows cancer cells to leave the primary tumor and metastasize. The loss of E-cadherin, a cell adhesion molecule, is a biomarker of EMT [5]. NetworkProfiler identified 25 key regulators of E-cadherin, of which half have been previously described and the other half were novel candidates. NetworkProfiler also revealed regulatory changes in *miR-141*, *ZEB1*, and E-cadherin. Specifically, our results suggested that decreased expression of *miR-141* in mesenchymal cells disrupts the negative feedback loop between *miR-141* and *ZEB1*, which would allow *ZEB1* to decrease the expression of E-cadherin during the EMT. In addition, we predicted 45 EMT-dependent putative master regulators that control sets of genes involved in cell adhesion, migration, invasion and metastasis, namely, 17 of which are downstream targets of TGFB1, a master switch of the EMT. To further validate the performance of NetworkProfiler, we experimentally evaluated *in silico* predictions obtained by NetworkProfiler. We consequently found that knockdown of KLF5, a new candidate regulator of E-cadherin, decreased E-cadherin expression and induced morphological changes characteristic of EMT. In addition, the functional involvement of miR-100 was validated in some EMT-related aspects, which was consistent with the predictions obtained by Network Profiler.

Results

Overview of NetworkProfiler

Here, we provide an overview of NetworkProfiler; please refer to the Methods section for a complete description. NetworkProfiler is a modulator-dependent graphical model because it includes a modulator (M) variable in addition to regulator (R) and target (T) variables (genes). R controls the transcription of T and M is a cofactor that modulates the interaction between R and T. In this study, we defined M as a biological or a clinical feature that is related to cancer, such as drug response, survival risk, or a molecule or pathway that is related to cancer initiation, progression, or metastasis. The relationships between R, T, and M are illustrated in Figure 1a. As shown in Figure 1b, the strength of the relationship between R and T varies depending on the value of M. Thus, M does not affect R and T directly; instead, it influences the strength of the relationship between R and T. In contrast, existing graphical models, such as Bayesian networks and mutual information networks [4], do not consider the effect of M (Figure 1c), so the strength of the relationship between R and T remains constant for all values of M (Figure 1d).

In addition, NetworkProfiler can infer the relationships between R and T, given a value of M. As a result, we could use NetworkProfiler to construct patient-specific networks with varying R-T relationships that reflect changes in the feature of interest in cancer patients. A simple example with synthetic data for R, T, and M is shown in Figure 2a. In this example, we assume that R regulates T only with a high value of M (Figure 2b). In this case, most existing methods that only consider R and T in all of the samples (Figure 2c) and ignore M would conclude that R does not regulate T. In contrast, NetworkProfiler attempts to quantify the strength of the relationship between R and T for a specific value m of M by reweighting the data according to the value of M to identify the neighborhood of samples with values of M that are close to m. Then, NetworkProfiler measures the dependency between R and T on the basis of these neighboring samples. The optimization of the size of the neighborhood is explained in the Method section.

A schematic representation of the entire analytical process of NetworkProfiler is shown in Figure 3. NetworkProfiler used 2 inputs: (1) gene expression data and (2) the modulator for each sample (Figure 3a). The gene expression data was represented as a $p \times n$ matrix, where p is the number of genes and n is the number

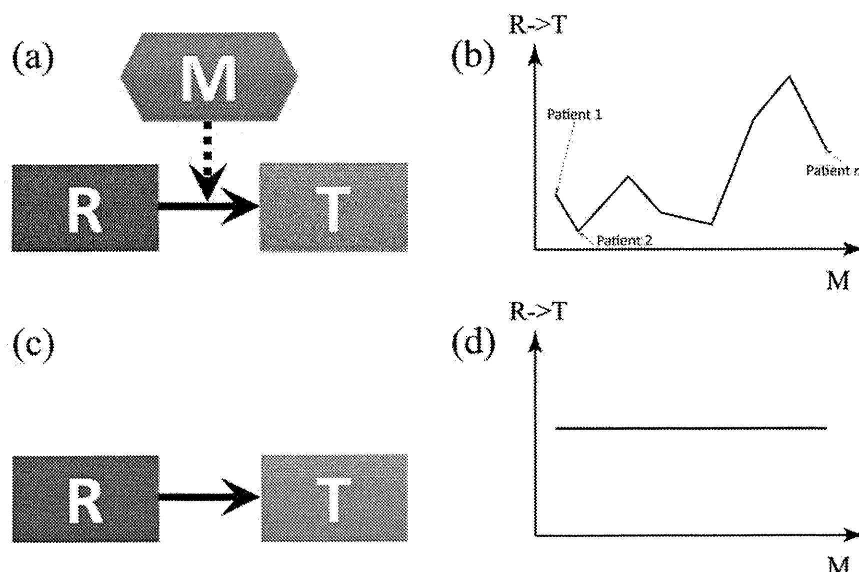

Figure 1. The relationships between a regulator (R), a target(T), and a modulator (M) in NetworkProfiler and existing graphical models. (a). The relationships between R, T and M in NetworkProfiler. The directed solid-line edge from R to T represents "R regulates the transcript of T". The directed dot-line edge from M to the edge between R and T describes "M controls the strength of the relationship between R and T". (b). The strength of the relationship between R and T in NetworkProfiler that varies depending on the value of M. (c). The relationships between R and T in existing graphical models that do not consider the effect of M. (d). The strength of the relationship between R and T in existing graphical models that remains constant for all values of M.
doi:10.1371/journal.pone.0020804.g001

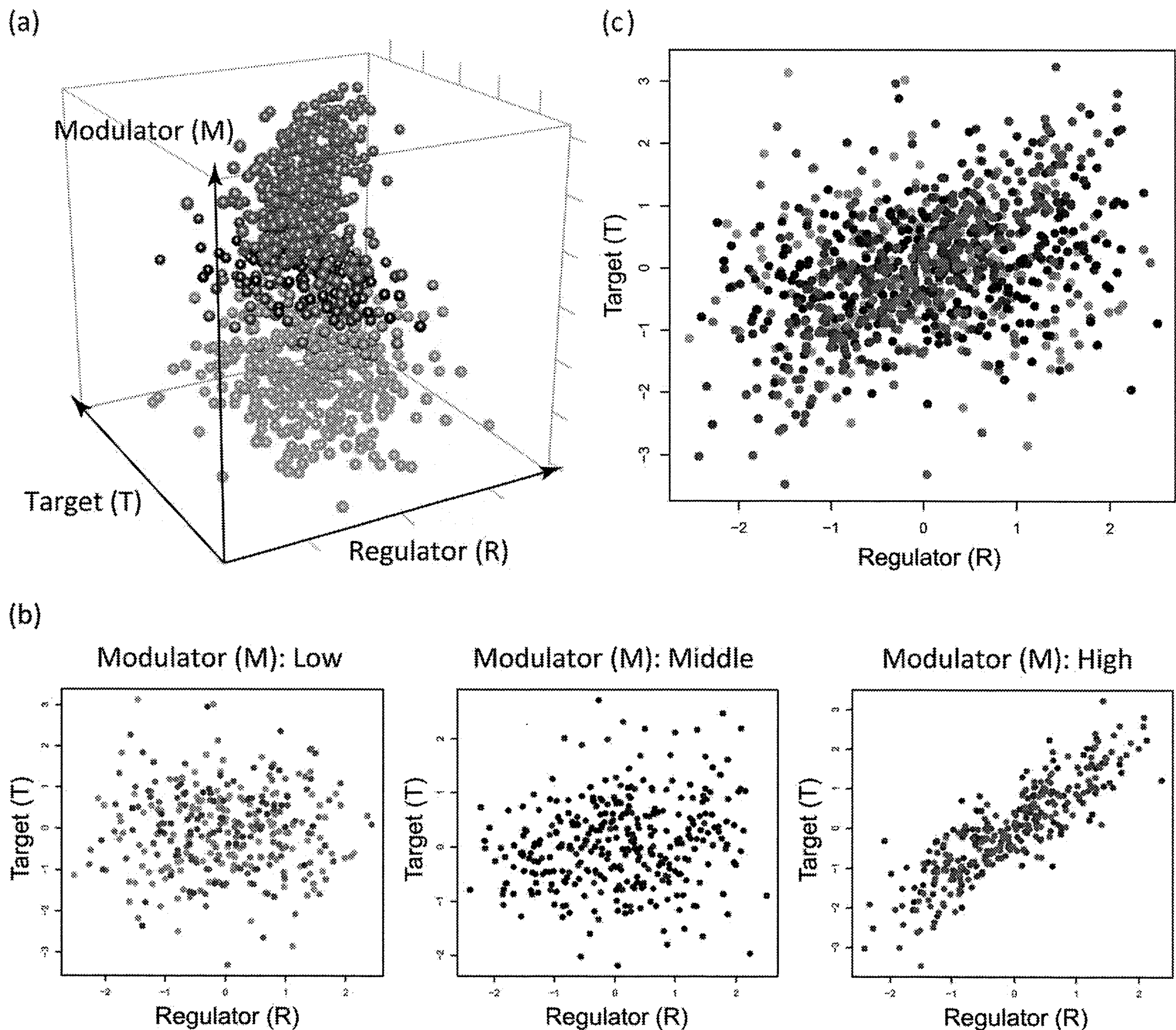

Figure 2. A regulatory change between a regulator (*R*) and a target (*T*) depending on the value of a modulator *M*. (a). A simple example with synthetic data from 1000 samples for *R*, *T*, and *M* where *x*-, *y*-, and *z*-axises correspond to the expressions of *R* and *T*, and the values of *M*, respectively. (b). The 3 scatter plots of *R* and *T* that are conditioned on the value of *M*. The left, middle, and right figures represent the scatter plots from 1-st sample to 333-th sample, from 334-th sample to 666-th sample, and from 667-th sample to 1000-th sample in order of ascending *M*, respectively. (c). The scatter plot of *R* and *T* that are not conditioned on the value of *M*.
doi:10.1371/journal.pone.0020804.g002

of samples (patients). If the modulator was an observable variable, then we directly applied NetworkProfiler to these inputs. However, if the modulator was a variable that is difficult to observe, then we used a signature-based hidden modulator extraction algorithm to estimate the value of the modulator. The output of NetworkProfiler is a set of gene networks for every value of *M* (i.e., sample-specific gene networks) shown in Figure 3b.

Afterwards, we used 2 post-analysis techniques to extract biological information from the networks. The first technique identified upstream regulators of a target gene of interest in the constructed modulator-dependent gene networks. To evaluate the modulator-dependent strength of a regulator for the target gene, we created a measure called the regulatory effect. The regulatory effect profiles of the upstream regulators for specific target genes are shown in Figure 3c. The second technique discovered putative master regulators that control downstream target gene sets with previously curated functions. To evaluate the enrichment of the target genes on a functional gene set, we created measure called the enrichment score. The resulting regulator-function matrix (Figure 3d) illustrates the candidate regulators (rows) of functions (columns) that are enhanced in the target genes.

Identification of system changes in the epithelial-mesenchymal transition

To identify system changes during the EMT, we applied NetworkProfiler to gene expression profiles of 762 cancer cell lines from the Sanger Cell Line Project (http://www.broadinstitute.org/cgi-bin/cancer/datasets.cgi). This dataset included the expression profiles of 22,777 probes, which correspond to 13,006 mRNAs in these cancer cell lines from the Affymetrix GeneChip

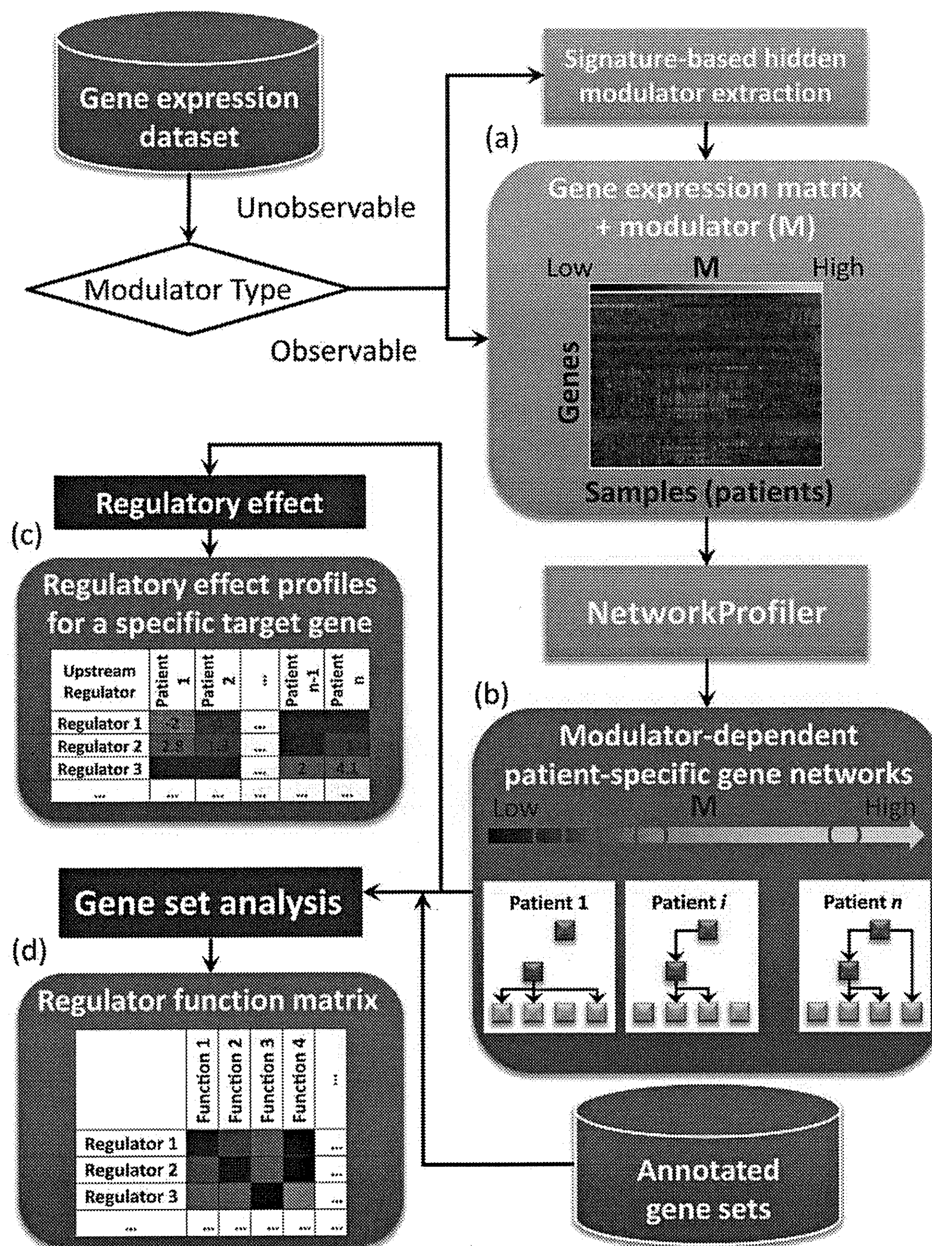

Figure 3. A schematic representation of the entire analytical process of NetworkProfiler. (a). Inputs of NetworkProfiler: gene expression data matrix and the modulator for each sample. (b). Outputs of NetworkProfiler: a set of gene networks for every value of M (i.e., sample-specific gene networks). (c). The regulatory effect profiles of the upstream regulators for a specific target gene. (d). The resulting regulator function matrix whose columns are the candidate regulators and rows are functions that are enhanced in the target genes.
doi:10.1371/journal.pone.0020804.g003

Human Genome U133 Array Set (HG-U133A) and the expression profiles of 502 human microRNAs from bead-based oligonucleotide arrays. The MAS5-normalized mRNA dataset was further transformed to the log scale and quantile-normalized. During the mapping of the probes to genes, we selected 1 probe for each gene that had the largest variance, which produced a final 13,508 (genes) × 762 (cancer cell lines) gene expression matrix.

In this study, we considered transcription factors, nuclear receptors, and microRNAs to be potential regulators. To identify transcription factors and nuclear receptors, we selected human genes that were annotated as a "transcription regulator" or "ligand-dependent nuclear receptor" from the Ingenuity Knowledge Base (IKB; http://www.ingenuity.com). We also included some transcription factors that were not annotated in the IKB but were annotated in the Biobase Knowledge Library (BKL; http://biobase-international.com/). We mapped a total of 1230 genes in the HG-U133A microarray gene set to 1183 transcription factors and 47 nuclear receptors (Table S1). In addition, we included 502 human miRNA probes (Table S2).

To calculate the modulator values for the EMT in the 762 cancer cell lines, we applied a signature-based hidden modulator extraction algorithm (see Methods for details) to the expression data. First, we selected 122 genes labeled "EMT_UP", "EMT_DN", "JECHLINGER_EMT_UP", and "JECHLINGER_EMT_DN" from Molecular Signatures Database v2.5 ([6]; http://www.broadinstitute.org/gsea/msigdb/index.jsp). Then, this algorithm narrowed the set to

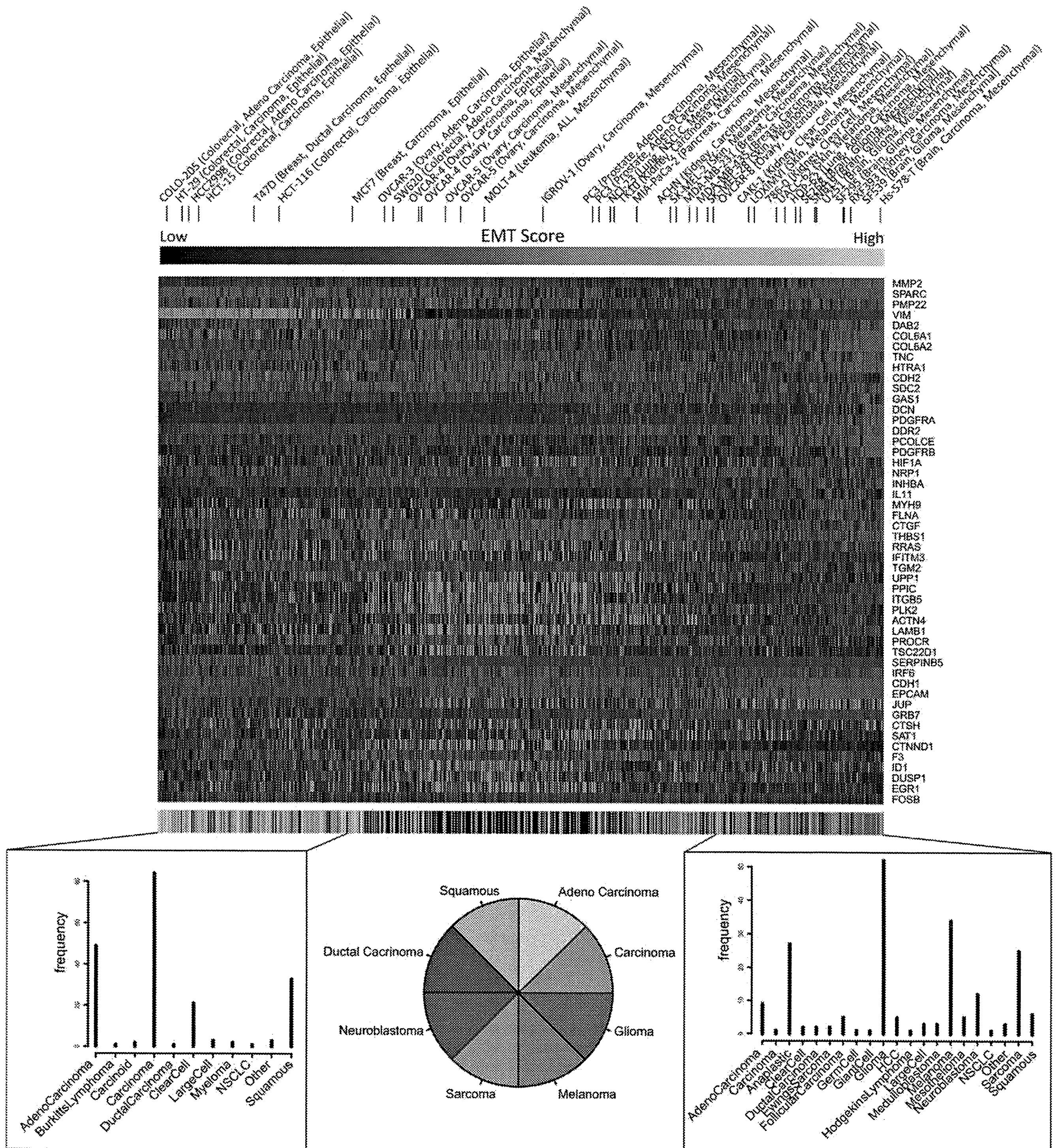

Figure 4. Expression profiles of the 50 functionally coherent genes in ascending order of the EMT-related modulator values. The heatmap represents normalized expression profiles so that the mean and variance for each gene are 0 and 1, respectively. The red color represents positive expressions and the green color represents negative expressions. The upper strings indicate cell line names which are known to be epithelial or mesenchymal. The upper horizontal color bar represents the values of the EMT-related modulator with the signature-based hidden modulator extraction algorithm. The bottom horizontal color bar shows primary histories of 762 cancer cell lines whose color corresponds to one of the eight primary histories or the other histories (black). The bottom histograms represent frequencies of the primary histories between samples with the 200 lowest and 200 highest values of the EMT-related modulator, respectively.
doi:10.1371/journal.pone.0020804.g004

50 functionally coherent genes with $p<10^{-5}$ by using the extraction of expression module (EEM) [7] (Table S3) and computed the first principal component of these 50 genes as hidden values of the EMT-related modulator (Table S4). Since the direction of the first principal component did not always correspond to that of the EMT, we changed the sign of the modulator values by

multiplying either plus or minus one so that epithelial-like cells have lower modulator values than mesenchymal-like cells.

Figure 4 shows the expression profiles of the 50 functionally coherent genes in ascending order of the EMT-related modulator values. These modulator values clearly discriminated cell lines that were epithelial-like or mesenchymal-like. Specifically, cells with smaller or larger modulator values had more epithelial or mesenchymal phenotypes, respectively. Furthermore, many carcinomas and squamous tumors had low modulator values, while many gliomas and melanomas had high values. By using these EMT-related modulator values, NetworkProfiler constructed 762 regulatory gene networks that are related to the EMT. The list of the estimated edges in each of these networks can be downloaded from the supporting web site (Files S1, S2, and S3; http://bonsai.hgc.jp/~shima/NetworkProfiler).

Identification of regulators of E-cadherin that induce the epithelial-mesenchymal transition

To identify possible regulators that might control the expression of E-cadherin during the EMT, we calculated the regulatory effects of the upstream regulators of E-cadherin. Out of 1732 potential regulators, NetworkProfiler inferred that 370 of them may control the expression of E-cadherin in any of the 762 cancer cell lines (Table S5). These putative regulators were ranked according to the change in their regulatory effect during the EMT. Although we did not include any information on known E-cadherin regulators, about half of the 25 highest ranked regulators were previously reported in the literature (Table 1). For example, 2 zinc finger transcription factors, ZEB1 and ZEB2, are direct repressors of E-cadherin and are involved in the EMT [9,15]. In addition, the miR-200 family indirectly suppresses the EMT by inhibiting the translation of ZEB1 and ZEB2 mRNAs [8]. Similarly, miR-192 inhibits the translation of ZEB2 [13,14]. In addition, SNAI2, a member of the Snail superfamily of zinc finger transcription factors, also is involved in the EMT [16]. Likewise, TCF4 (also known as E2-2), a class I bHLH transcription factor, is an EMT regulator; its isoforms induce the EMT in MDCK kidney epithelial cells [12]. In contrast, FOXA1 and FOXA2 are positive regulators of E-cadherin, which suppress the EMT in pancreatic ductal adenocarcinoma [11]. KLF4 also inhibits the EMT by regulating E-cadherin expression [10]. NetworkProfiler also identified several other known direct repressors of E-cadherin, such as TWIST1 [17] and TCF3 (also known as E47) [18]; however, these regulators were ranked 38th and 84th, respectively.

The other half of the 25 highest ranked regulators has not yet been reported and may be novel EMT-dependent regulators of E-cadherin. For example, although the relationship between GRHL2 and EMT is not known, GRHL2 is required for morphogenesis of epidermal and tracheal cells and plays an important role in regulating the expression levels of E-cadherin in *Drosophila* post-embryonic neuroblasts [19]. ZNF217 binds the E-cadherin promoter [20], which suggests that ZNF217 might be a transcription factor for E-cadherin.

Next, we compared the performance of NetworkProfiler with that of a structural equation model (SEM) of E-cadherin that was inferred by the elastic net [22]. This model was equivalent to a regression model where the response variable is the expression of E-cadherin and the explanatory variables are the 1732 regulator expressions. The significance of each regulator was evaluated based on the number of non-zero regression coefficients in 1000 bootstrapped datasets. The SEM inferred 627 putative regulators (Table S6). Among these putative regulators, there were only 6 regulators, namely, *ZEB1*, *miR-141*, *ZEB2*, *TCF3*, *miR-200b*, and *miR-200c*, in the 25 highest ranked regulators that were previously reported in the literature. This result suggested that NetworkProfiler was superior to the traditional gene network estimation methods to identify regulators of E-cadherin that are involved in the EMT. Moreover, NetworkProfiler can reveal regulatory changes among genes during the EMT. Figures 5a and 5b show the regulatory profiles of putative regulators of E-cadherin when the lengths of the paths from the regulators to E-cadherin is 1 and 2, respectively.

NetworkProfiler can also predict mechanistic interpretations of published experiments. For example, it is known that ZEB1 and ZEB2 induce EMT by repressing E-cadherin transcription and that ectopic expression of the miR-200 family (miR-200a, miR-200b, miR-200c, and miR-141) or miR-205 leads to downregulation of ZEB1 and ZEB2, upregulation of E-cadherin, and mesenchymal-epithelial transition (MET) in cells [8]. As the relationships between these genes, the prediction of NetworkProfiler provides the following results. As shown in Figures 6c and 6d, although the expression of miR-141 had a strong positive effect on that of E-cadherin in epithelial-like cells, this effect decreases during the EMT. In contrast, although the expression of ZEB1 had a weak negative effect on that of E-cadherin in epithelial-like cells, this effect increased during the EMT. Interestingly, miR-141 and ZEB1 had a strong, direct

Table 1. 25 top-ranked regulators of E-cadherin for the change in the regulatory effect change among the EMT with published evidence.

regulator	type	regulatory effect change	Evidence
IRF6	A	101.04	
miR-141	A	87.58	[8]
GRHL2	A	64.13	
ZEB1 (SIP1)	I	50.72	[9]
LSR	I	46.89	
miR-200b	A	31.55	[8]
KLF4	A	26.28	[10]
OVOL2	A	22.08	
miR-200a	A	17.70	[8]
FOXA2	A	17.26	[11]
TCF4 (E2.2)	I	14.15	[12]
ELF3	A	13.58	
ZNF217	A	13.53	
MYB	A	12.50	
KLF5	A	12.42	
miR-192	A	12.30	[13, 14]
FOXA1	A	11.69	[11]
ZNF165	A	11.39	
NKX2-1	A	11.21	
HNF1B	A	11.08	
TFE3	A	11.01	
ZEB2 (δEF)	I	10.66	[15]
TRIM29	I	9.87	
SNAI2	I	9.74	[16]

The labels "A" and "I" indicate 2 types of the regulator: activator (A) and inhibitor (I). See Table S5 for the complete table of the 370 putative regulators for E-cadherin.

doi:10.1371/journal.pone.0020804.t001

(a)

Low (Epithelial) EMT-related modulator High (Mesenchymal)

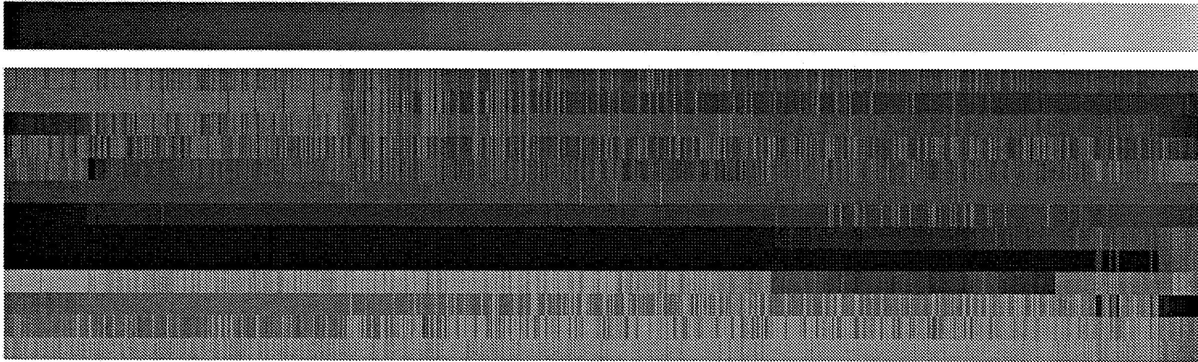

ELF3
miR-141
GRHL2
miR-135b
LSR
NAT8
miR-211
IRF6
OVOL2
TCF3
ZEB2
ZEB1
DAXX

(b)

Low (Epithelial) EMT-related modulator High (Mesenchymal)

367 grandparent regulators

Figure 5. Regulatory effect profiles of the putative regulators of E-cadherin among the EMT. (a). The regulatory effect profiles of the 13 putative regulators among the EMT when the length of the paths from the regulators to E-cadherin is 1 where rows indicate the putative regulators of E-cadherin and columns indicate samples (cancer cell lines). The positive (red) and negative (green) regulatory effect indicate that the parent regulator controls the transcript of E-cadherin positively and negatively, respectively. (b). The regulatory effect profiles of the 13 putative regulators among the EMT when the length of the paths from the regulators to E-cadherin is 2.
doi:10.1371/journal.pone.0020804.g005

negative effect on each other only when the EMT-related modulator values were low. This implied that there is a negative feedback loop between miR-141 and ZEB1 in epithelial-like cells, which is consistent with a previous study [23]. Furthermore, during the EMT, the expression levels of miR-141 and E-cadherin decreased, while the expression level of ZEB1

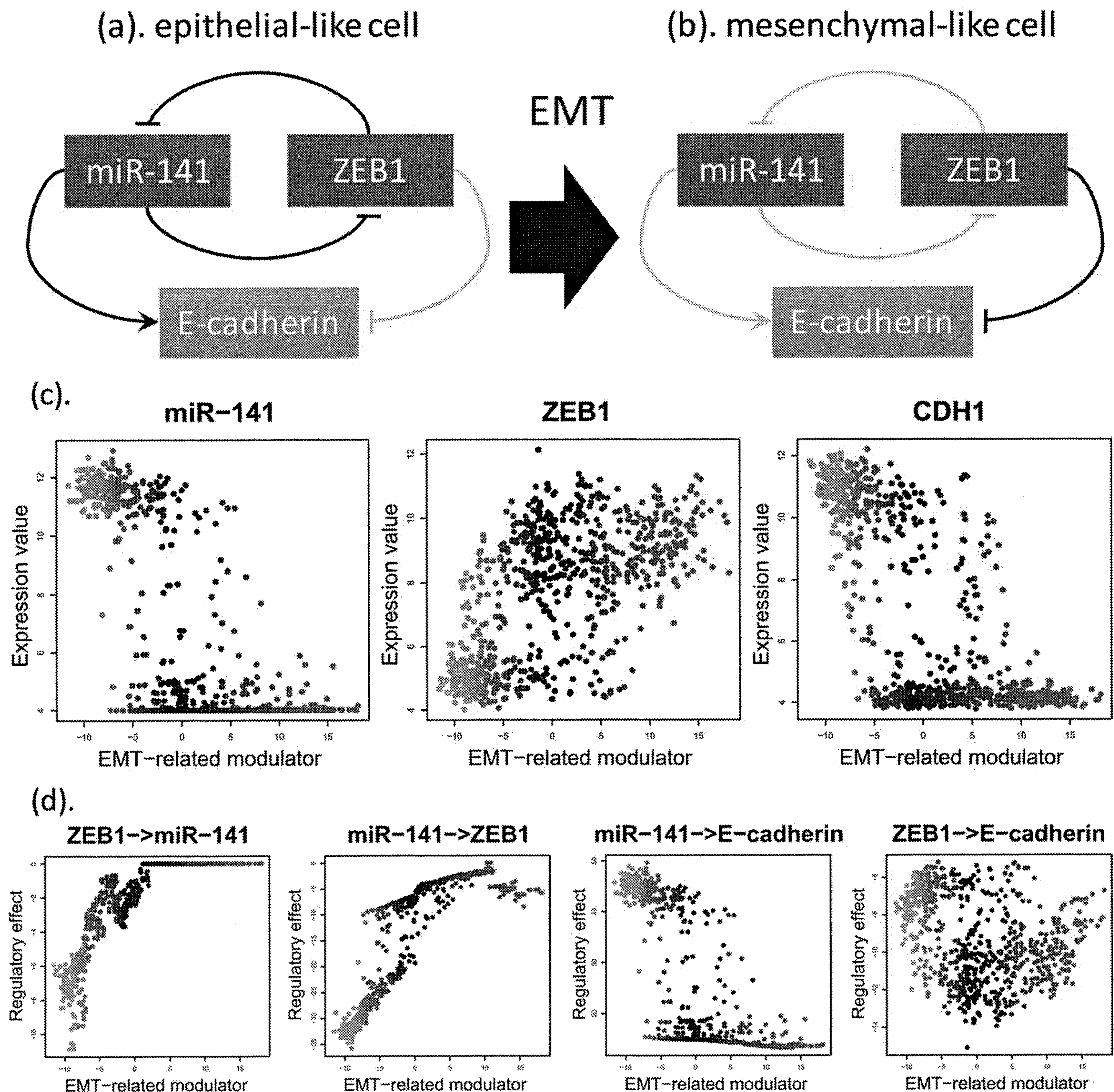

Figure 6. Regulatory changes among miR-141, ZEB1, and E-cadherin among the EMT. (a). The relationship among miR-141, ZEB1, and E-cadherin in epithelial-like cells. (b). The relationship among miR-141, ZEB1, and E-cadherin in mesenchymal-like cells. (c). The expression profiles of miR-141 (left), ZEB1 (middle), and E-cadherin (right) in order of ascending the EMT-related modulator values. The green and red colors indicate epithelial- and mesenchymal-like cells, respectively. (d). The regulatory effects from ZEB1 to miR-141, from miR-141 to ZEB1, from miR-141 to E-cadherin, and from ZEB1 to E-cadherin when the length of the paths is 1.
doi:10.1371/journal.pone.0020804.g006